Roughness evaluation of Ti6Al4V bulks produced by laser powder directed energy deposition and micro-milled for biomedical applications

Transactions on Additive Manufacturing Meets Medicine
Trans. AMMM, 2024, Vol. 6, No 1, Article ID 1799, 6 Pages

Infinite Science Publishing

Original Research Article

Roughness evaluation of Ti-6Al-4V bulks produced by laser powder-directed energy deposition and micro-milled for biomedical applications

V. Wong[1*], W. Valicelli[1], T. Monteiro[1], G. Ribeiro[1], A. Capaldo[2], and A. Rodrigues[1]

[1] *Mechanical Engineering Department, Sao Carlos School of Engineering, University of Sao Paulo, São Carlos, Brazil.*
[2] *Biotechnology and Tissue Engineering, Postgraduate Program in Biotechnology, University of Araraquara, Araraquara, São Paulo, Brazil.*
[*] *Corresponding author, email: vwong.ufs@gmail.com*

Abstract: Laser Powder-Directed Energy Deposition (LP-DED) has excelled as a technology that can produce parts with large dimensions in less time. Furthermore, the micro-milling process can be combined to provide a uniform surface and a high quality of roughness that directly impacts osteointegration and cellular adhesion. This paper aimed to manufacture bulks produced by LP-DED with two different powders and different laser powers. In sequence, the milling process was used to create six channels and evaluate the influence of the feed per tooth (f_z) on the bulk surface. The values obtained from the as-built bulks revealed the impact of the laser power and powder features on the surface of the bulks, obtaining values around 30-55 µm for the Sq and 20-45 µm for the Sa, respectively. These values were reduced when applying micro-milling from 1.0 to 1.5 µm in terms of Sa and 1.5 to 2.5 µm for the Sq. Regarding Skewness and Kurtosis, the results revealed Ssk > 0, indicating a surface with greater valley concentration, and in most cases, Sku > 3, describing the prevalence of sharp peaks or valleys. This surface microtopography can provide cell housing and form a bone matrix around the implant.

I. Introduction

With the emergence of metal Additive Manufacturing (AM), the medical industry has found a set of technologies that can simplify some of the challenges related to the manufacturing of biomedical components and devices, including orthopedic implants [1-3], dental implants [4][5], prostheses, and orthosis [6-8]. These technologies reduce production times and offer complex, patient-specific medical devices.

One of the key advantages is the individualized nature of the solutions provided by metal AM. These solutions are tailored to respect the unique characteristics of human bodies, the specific biomedical requirements, and the distinct disease patterns, offering a level of personalized care that was previously unattainable [9][10].

When the biomedical component is projected, the compatibility (mechanical, chemical, and biological) must be reached. Because of this, the feedstock, surface chemistry, and topography, including roughness and micro-texture, play an important role in guaranteeing wettability and cellular viability [11].

Zhu et al. highlighted that the wettability surface might be affected by the cells and the physicochemical linkages between the cells and the surface, such as ionic forces or due to the alterations in the absorption of conditioning molecules, including proteins [11].

Hacking et al. reported that when the surface is under shear conditions, the asperities on rougher surfaces improve the interlock between the adjacent bone tissue, and the surface also improves, increasing the resistance to mechanical disruption [12]. Previous studies also revealed that as wettability increases, the interaction between the component surface and the biological environment improves [11][13-16].

Trevisan et al., [17] Highlighted that osteoblastic cells adhesion, growth, and differentiation promote the integration of the implant with the bone tissue and are influenced by surface energy and surface roughness. They also pointed out that the porosity pore size, the amount of porosity, and the shape of the pores can also influence cell proliferation and differentiation [17-21].

Regarding the feedstock, Titanium alloys, Stainless Steel, and CoCr alloys are frequently used in biomedical applications [18]. Ti-6Al-4V is one of the most widely explored first-generation materials within titanium alloys due to its mechanical properties and corrosion resistance. In this alloy, Aluminium (Al) stabilizes and strengthens the α phase, increases α+β ↔ β transformation temperature, and reduces the alloy density. Vanadium (V) stabilizes the β phase, lowering the temperature required for this transformation [22].

The roughness in the metal AM processes powder-based is affected by the powder characteristics and process parameters [23-25]. The powder characteristics include the particle size distribution, chemical composition, powder morphology, density, and flow rate. In Laser Powder Directed Energy Deposition (LP-DED) and Powder Bed Fusion (PBF), the process parameters that affect the roughness include the build orientation, laser power, scan speed, hatch spacing, and layer thickness [25][26].

In both technologies, the surface is commonly characterized by the adherence of semi-melted powder, the stair phenomenon associated with the track geometry, and the appearance of pores or regions with incomplete melting. [27]. For this reason, a set of roughness parameters that represent the must be carefully selected. Moreover, postprocessing and surface finishing are commonly used in the literature to uniformize the surface in both PBF and LP-DED [27-29].

On average, the surface roughness obtained using the LP-DED process is three times higher than that obtained with PBF processes [30]. In contrast, according to Optomec, LP-DED can produce components ten times faster and five times less expensive than PBF [31][32]. Furthermore, when the volume of the component increases, some limitations regarding the build dimension could be identified. In sequence, the processing time increases. LP-DED could be more suitable for fabricating large-volume components for biomedical applications.

This paper aims to evaluate the evolution of roughness surface in parts produced by LP-DED and micro-milled to enable the cell viability test in vitro.

II. Materials and methods

II.I Metal powder

This research uses two powders to produce 15 x 15 x 10 mm^3 bulks. The first powder was a Ti6Al4V Grade 5 powder produced by Advanced Plasma Atomization (APATM) and provided by AP&C Powder Metallurgy. The second powder was a Ti6Al4V Grade 23 made by a gas atomization process and provided by Carpenter Additive. A sample of both powders was extracted, and metallography was prepared. A confocal microscope LEXT Olympus OLS 4100 was used to assess dimensional and morphological features.

II.II Experimental setup

The LP-DED machine used in this experiment is a BeAM Machines Modulo 250 equipped with a Ytterbium fiber laser with 1 kW of maximum laser power produced by the IPG Fiber Laser with a Gaussian spot size of ~ 60 µm. The main process parameters used in this experiment are summarized in Table 1.

Table 1. Process parameters selected.

Process Parameters	Values
Laser Power (W)	300 - 315 - 330 - 345
Powder Feed Rate (g/min)	5.4
Scanning Speed (mm/min)	2000
Shield gas (l/min)	6
Central gas (l/min)	3
Carrier gas (l/min)	3

All the experiments were conducted under an inert atmosphere using argon as an inert gas.

II.III Micro-milling setup

The machine center used in this experiment is a ROMI model D600 embedded with a high rotation motor spindle Nakanishi model NR3060S. An endmill of Ø 32 mm, with a depth of cut of 0.25 mm, cutting speed of 50 m/min, and feed per tooth of fz = 0.050 mm/tooth, was used to uniformize the surface of the bulks. In sequence, six channels were milled in each bulk. Each micro-channel was composed of three adjacent straight passes on each channel by considering feed per tooth f_z = 12 µm/tooth for the 330 W and f_z = 24 µm/tooth for the 345 W, depth of cut a_p = 30 µm, width of cut a_e = 300 µm, up-milling strategy, 15,280 rpm, and no cutting fluid. Endmills with two flutes and diameter d_f = 500 µm produced by Mitsubishi were employed (MS2MSD0050 specification). A new tool was used for each sample. The process parameters adopted in this study are based on the results obtained in previous studies [33].

II.III Sample characterization

The bulks were cleaned with acetone under ultrasonic vibration at 35 kHz using a sonicator machine, Julabo USR 1, to remove particles adhering to the study surface. The confocal microscope, LEXT Olympus OLS 4100, was used to evaluate the bulk roughness before and after the micro-

milling process. Fig. 1 summarizes the proposed methodology used in this paper.

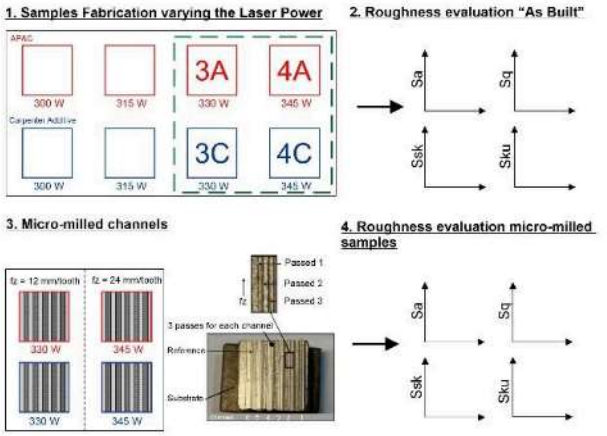

Figure 1. Workflow of the proposed methodology

The roughness parameters selected for surface analysis of the bulks were Arithmetical Mean Height (Sa) Eq. 1, Root Mean Square Height (Sq) Eq. 2, Skewness (Ssk) Eq. 3, and Kurtosis (Sku) Eq. 4.

$$S_a = \frac{1}{A}\int_A |Z(x,y)|\, dxdy \quad (1)$$

$$S_q = \sqrt{\frac{1}{A}\iint_A Z^2(x,y)dxdy} \quad (2)$$

$$S_{sk} = \frac{1}{S_q{}^3}\left(\frac{1}{A}\iint_A Z^3(x,y)\, dxdy\right) \quad (3)$$

$$S_{su} = \frac{1}{S_q{}^4}\left(\frac{1}{A}\iint_A Z^4(x,y)\, dxdy\right) \quad (4)$$

Other studies have used these parameters for their relevance to surface evaluation [34-36]. Three analysis areas were selected at the microchannels: beginning (a), middle (b), and end (c). Lastly, the roughness parameters were extracted, and the results were discussed.

III. Results and discussions

III.I Particle size distribution and morphology

The cross-section micrograph of both powders revealed particles predominantly spherics, as reported in Fig. 2. Irregular shapes, satellites, flakes, and pores in fewer extensions were observed in the powder provided by Carpenter A., as reported in Fig. 2a.

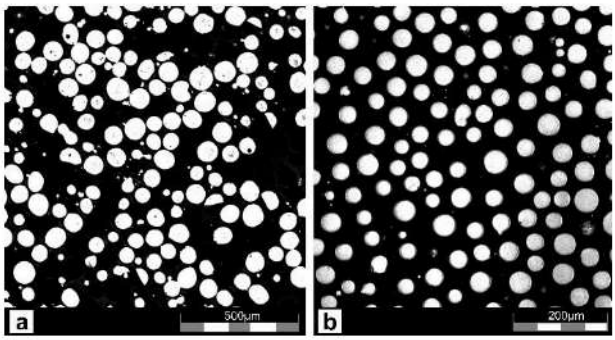

Figure 2. Powder cross-section micrograph of a) Carpenter Additive, b) AP&C powder.

The micrograph of the powder supplied by AP&C revealed predominantly spheric particles, as shown in Fig. 2b. The d10, d50, and d90 are reported in Table 2. The particle size distribution of both powders is presented in Fig. 3.

The range obtained for the Carpenter additive described values between 20 and 100 µm. Instead, the range obtained for the AP&C powder was between 30 and 70 µm. Both powders describe an unimodal curve.

Table 2. d10, d50, and d90 values for both powders.

	d10 (µm)	d50 (µm)	d90 (µm)
Carpenter A.	54.74	71.43	88.37
AP&C	38.98	47.24	54.60

From the PSD, the percentual frequency in the powder provided by AP&C slightly increased, indicating a greater number of particles concentrated around the mean value.

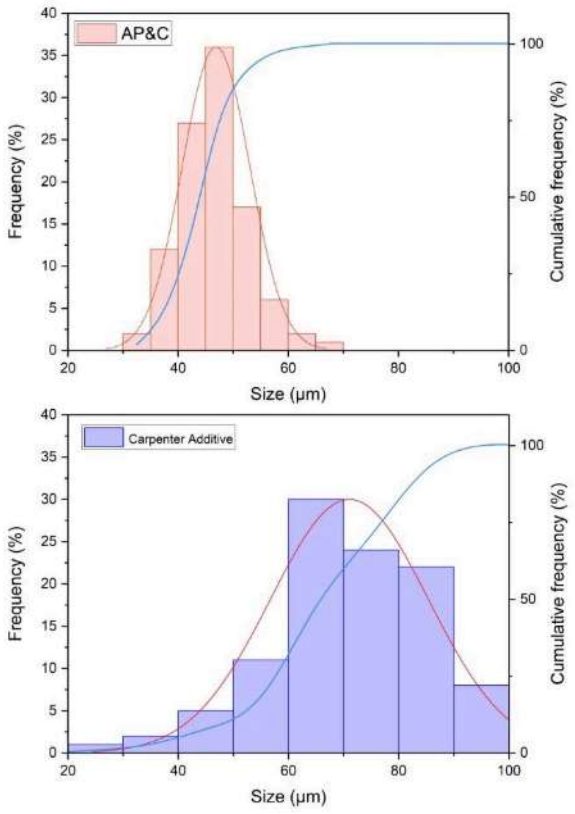

Figure 3. Particle Size distribution of the Ti-6Al-4V

The results obtained from this analysis are important for correlating the influence of the Laser Power and geometrical features with the bulk roughness (as built).

III.II Roughness analysis (as-built)

Height roughness parameters, including Sa and Sq, were measured in the bulks (As-built) at the plane XY center top. From this analysis, it was possible to observe that as the laser power increased, both values Sa and Sq decreased, and the values for both powders were also clearly distinguishable, as described in Fig. 4.

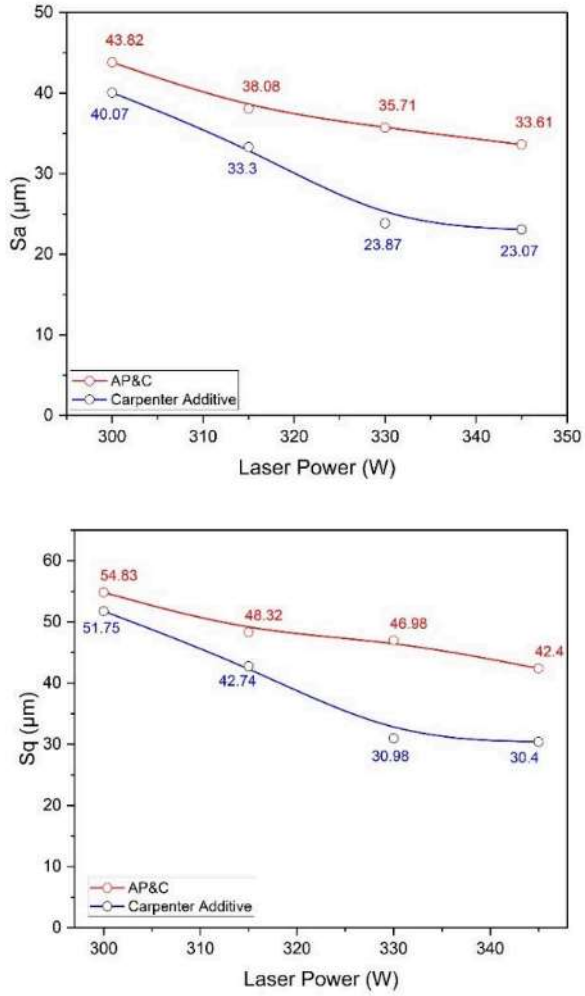

Figure 4. Sa and Sq values of the as-built samples

These findings were also observed in the research developed by Jardon et al., where smaller particles reduced roughness, resulting in better surface finishing [29]. However, the roughness values obtained for both powders cannot be directly compared because the powder feed rate and the laser power affect the geometry and microstructure of the track differently.

On the other hand, as the particles' dimensions increase, unmolten particles can appear. The increment of the laser power provided energy to melt these particles, consequently reducing the surface roughness. The values obtained in this analysis were close to those obtained in the study developed by Peng et al., [36], with Sa values between 25 µm and 28.5 µm for the heat-untreated samples and between 27 µm and 31 µm for the samples with heat treatment, and in terms of Sq values between 31 µm and 35 µm for the heat-untreated and between 33 and 37.9 µm for the heat-treated samples.

Regarding the Skewness, Ssk revealed values with a positive asymmetry (Ssk>0), as illustrated in Fig. 5. The values of Ssk obtained in this analysis were close to those obtained in the study developed by Peng et al., [36]. Values between 0.01 and 0.51 for the heat-treated and 0.5 to 0.78 for the untreated samples, indicating a surface with round valleys and sharp peaks, enabling the possibility of the cellular adhesion test.

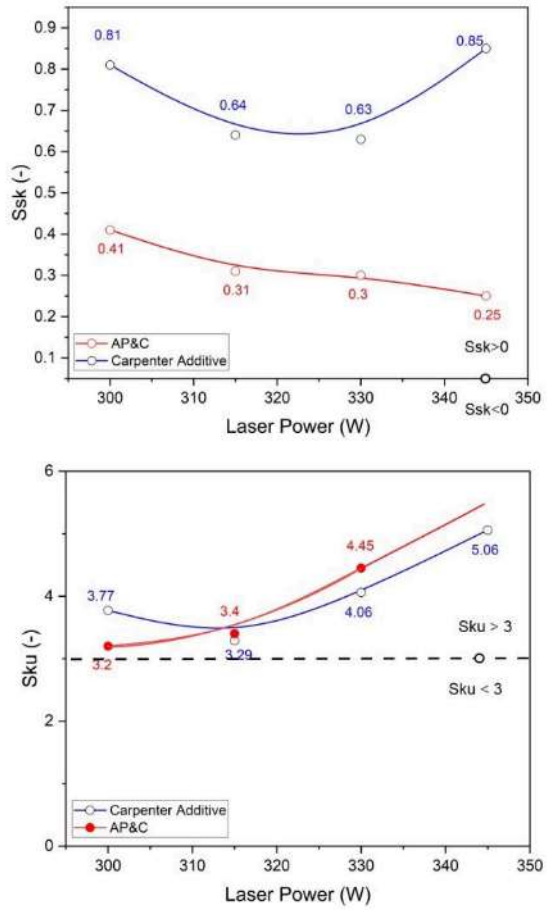

Figure 5. Influence of LP in the Ssk and Sku (As built)

Kurtosis revealed a leptokurtic behavior with (Sku>3), indicating a predominance of sharp peaks. In both cases, the Sku tended to increase, describing the nature of the surface quality provided by this process.

III.II Roughness analysis (micro-milled).

Once the channels were micro-milled, their beginning (a), middle (b), and end (c) were analyzed. In both cases, the values of Sa and Sq for the bulk 3C and 4C with fz = 12 µm/tooth and fz = 24 µm/tooth were slightly greater than those observed in bulks 3A and 4A. The values of Sa, Sq, and Ssk are described in Fig. 6. From the topographical point of view, the bulks 3C revealed burrs on the upper border of the channels, and 3A presented the same formation but in a lesser proportion, as shown in Fig. 7d.

Instead, the bulks 4A and 4C did not reveal the same burr formations. This phenomenon could be related to the formation of minimum chip thickness, as described in previous studies [33]. However, further investigation will focus on studying this phenomenon in depth.

Regarding the topographical evaluation, pores were also observed in Fig. 8b, especially in samples 3C and 4C. This could be because the feedstock pores that are transferred to

the melt pool, captured by solidification, and frozen into the deposition [37]; when micro-milling fabrication is applied, these oxides are visible at the floor of the micro-channel, with a geometry directly correlated with the geometry of the pore observed in the powder characterization. However, chemical analysis, including X-ray photoelectron spectroscopy, could provide more information about the surface's chemical composition and identify the built-up cutting-edge phenomena.

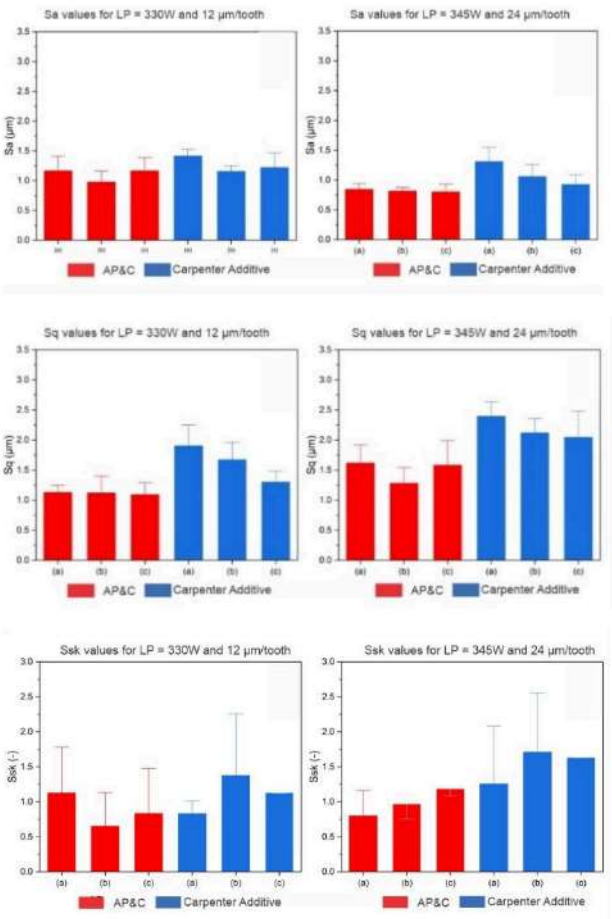

Figure 6. Sa, Sq, and Ssk plots of the surface micro-milled.

The skewness obtained revealed positive values (Ssk>0), meaning a surface with round valleys and sharp peaks. [33]. Regarding the kurtosis, values greater than three (Sku>3) were obtained for the 3A and 3C, as shown in Fig. 7a.

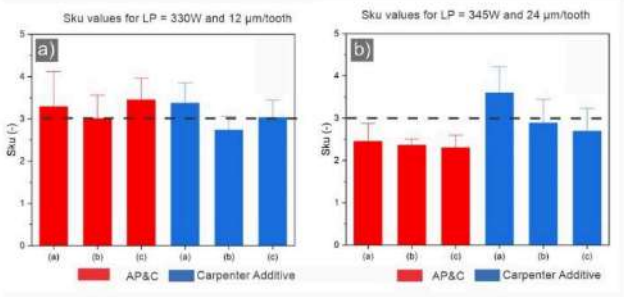

Figure 7. Kurtosis values for a) 3A – 3C, b) 4A – 4C.

Instead, the values obtained from the bulk 4A 4C were (Sku<3), indicating a platykurtic surface characterized by relatively few high peaks and low valleys that could be for the apparition of speed marks, as illustrated in Fig. 8a.

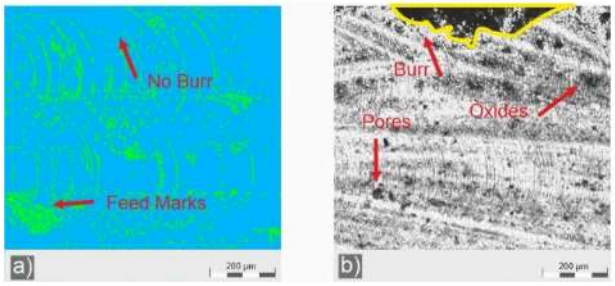

Figure 8. Evaluation of the bulk, a) 4A revealing feed marks, and b) 3A revealing burrs and oxides.

This surface texture produced by LP-DED and micro-milled can be interesting when applied to implants. A spiky topography (Sku > 0) with a predominance of peaks (Ssk > 3) could work as cell housing, maximize their attachment at microscope level, and, consequently, form a bone matrix around the implant.

IV. Conclusions

This research evaluated the evolution of the surface roughness in parts produced by LP-DED and then micro-milled with interest in biomedical applications. Based on the results obtained, the following conclusions can be drawn.

The increment of the laser power directly affected the surface topography by decreasing Sa, Sq, Ssk, and Sku.

The powder morphology plays a crucial role in reducing surface roughness. This finding provides valuable insights into the potential for surface refinement in medical applications.

Regarding Skewness and Kurtosis, the values obtained for LP-DED and the micro-milling process indicate that the surface obtained is useful for evaluating cellular viability (propagation, differentiation, and adhesion). Skewness is positive, and kurtosis is greater than 3, meaning sharp peaks are prevalent.

Acknowledgments

This Research was financed in part by the Coordination for the Improvement of Higher Education Personnel (CAPES), Finance Code 001, the National Council for Scientific and Technological Development (CNPQ), and the São Paulo Research Foundation (FAPESP). The authors would like to acknowledge Rodrigo Ferreira's contributions to the research field; his research enables the advancement of this research.

Author's Statement

Conflict of interest: The authors declare that they have no known competing financial interests or personal relationships that could have appeared to influence the work reported in this paper.

References

[1] T. Kim, C. W. See, X. Li, and D. Zhu, "Orthopedic implants and devices for bone fractures and defects: Past, present and perspective," Engineered Regeneration, vol. 1, pp. 6–18, 2020, doi: 10.1016/j.engreg.2020.05.003.

[2] G. Li et al., "In vitro and in vivo study of additive manufactured porous Ti6Al4V scaffolds for repairing bone defects," Sci Rep, vol. 6, no. 1, p. 34072, Sep. 2016, doi: 10.1038/srep34072.

[3] M. Tamaddon, S. Samizadeh, L. Wang, G. Blunn, and C. Liu, "Intrinsic Osteoinductivity of Porous Titanium Scaffold for Bone Tissue Engineering," Int J Biomater, vol. 2017, pp. 1–11, 2017, doi: 10.1155/2017/5093063.
[4] M. E. Onder et al., "Biomimetic dental implant production using selective laser powder bed fusion melting: In-vitro results," J Mech Behav Biomed Mater, vol. 151, p. 106360, Mar. 2024, doi: 10.1016/j.jmbbm.2023.106360.
[5] Z. J. Wally, A. M. Haque, A. Feteira, F. Claeyssens, R. Goodall, and G. C. Reilly, "Selective laser melting processed Ti6Al4V lattices with graded porosities for dental applications," J Mech Behav Biomed Mater, vol. 90, pp. 20–29, Feb. 2019, doi: 10.1016/j.jmbbm.2018.08.047.
[6] Q. Han et al., "Individual resection and reconstruction of pelvic tumor with three-dimensional printed customized hemi-pelvic prosthesis," Medicine, vol. 98, no. 36, p. e16658, Sep. 2019, doi: 10.1097/MD.0000000000016658.
[7] S. Savsani, S. Singh, and H. S. Mali, "Additive manufacturing for prostheses development: state of the art," Rapid Prototyp J, vol. 29, no. 4, pp. 741–765, Apr. 2023, doi: 10.1108/RPJ-01-2022-0029.
[8] S. Singh and S. Ramakrishna, "Biomedical applications of additive manufacturing: Present and future," Curr Opin Biomed Eng, vol. 2, pp. 105–115, Jun. 2017, doi: 10.1016/j.cobme.2017.05.006.
[9] K. Yandell, "Organs on demand," Science (1979), vol. 27, pp. 38–45, Sep. 2013.
[10] D. Omidvarkarjan, R. Rosenbauer, C. Klahn, and M. Meboldt, "Implementation of Additive Manufacturing in Industry," 2023, pp. 55–71. doi: 10.1007/978-3-031-20752-5_4.
[11] X. Zhu, J. Chen, L. Scheideler, R. Reichl, and J. Geis-Gerstorfer, "Effects of topography and composition of titanium surface oxides on osteoblast responses," Biomaterials, vol. 25, no. 18, pp. 4087–4103, Aug. 2004, doi: 10.1016/j.biomaterials.2003.11.011.
[12] S. A. Hacking et al., "Surface roughness enhances the osseointegration of titanium headposts in non-human primates," J Neurosci Methods, vol. 211, no. 2, pp. 237–244, Nov. 2012, doi: 10.1016/j.jneumeth.2012.09.002.
[13] S.C Dexter, "Influence of substratum critical surface tension on bacteria adhesion-in situ studies," J Colloid Interface Sci., vol. 70, pp. 346–354, 1979.
[14] RE Baier, EG Shafrin, and WA Zisman, "Adhesion: mechanisms that assist or impede it." Science (1979), vol. 162, pp. 1360–1368, Dec. 1968.
[15] M.E Schrader, "On adhesion of biological substances to low energy solid surface," J Colloid Interface Sci, vol. 88, pp. 296–297, 1982.
[16] R.E Baier, A.E Meyer, J.R Natiella, R.R Natiella, and J.M Carter, "Surface properties determine bioadhesive outcomes: methods and results," J Biomed Mater Res., vol. 18, pp. 337–355, 1984.
[17] F. Trevisan et al., "Additive manufacturing of titanium alloys in the biomedical field: processes, properties and applications," J Appl Biomater Funct Mater, vol. 16, no. 2, pp. 57–67, Apr. 2018, doi: 10.5301/jabfm.5000371.
[18] Bin Hasib H, "Mechanical behavior of non-stochastic Ti-6Al-4V cellular structures produced via electron beam melting (EBM)," North Carolina State University, Raleigh, 2011.
[19] J. E. Biemond, G. Hannink, N. Verdonschot, and P. Buma, "The effect of E-beam engineered surface structures on attachment, proliferation, and differentiation of human mesenchymal stem cells," Biomed Mater Eng, vol. 21, no. 5–6, pp. 271–279, 2011, doi: 10.3233/BME-2012-0675.
[20] S. Van Bael et al., "The effect of pore geometry on the in vitro biological behavior of human periosteum-derived cells seeded on selective laser-melted Ti6Al4V bone scaffolds," Acta Biomater, vol. 8, no. 7, pp. 2824–2834, Jul. 2012, doi: 10.1016/j.actbio.2012.04.001.
[21] B. R. Levine, S. Sporer, R. A. Poggie, C. J. Della Valle, and J. J. Jacobs, "Experimental and clinical performance of porous tantalum in orthopedic surgery," Biomaterials, vol. 27, no. 27, pp. 4671–4681, Sep. 2006, doi: 10.1016/j.biomaterials.2006.04.041.
[22] J. Sieniawski, W. Ziaja, K. Kubiak, and M. Motyk, "Microstructure and Mechanical Properties of High Strength Two-Phase Titanium Alloys," in Titanium Alloys - Advances in Properties Control, InTech, 2013. doi: 10.5772/56197.
[23] L. C. B. Carolo and R. E. Cooper O., "A review on the influence of process variables on the surface roughness of Ti-6Al-4V by electron beam powder bed fusion," Addit Manuf, vol. 59, p. 103103, Nov. 2022, doi: 10.1016/j.addma.2022.103103.
[24] Z. Jardon, J. Ertveldt, R. Lecluyse, M. Hinderdael, and L. Pyl, "Directed Energy Deposition roughness mitigation through laser remelting," Procedia CIRP, vol. 111, pp. 180–184, 2022, doi: 10.1016/j.procir.2022.08.042.
[25] M. N. Doğu, M. A. Obeidi, H. Gu, C. Teng, and D. Brabazon, "Powder Bed Fusion–Laser Beam of IN939: The Effect of Process Parameters on the Relative Density, Defect Formation, Surface Roughness and Microstructure," Materials, vol. 17, no. 13, p. 3324, Jul. 2024, doi: 10.3390/ma17133324.
[26] M. A. Obeidi, "Metal additive manufacturing by laser-powder bed fusion:Guidelines for process optimisation," Results in Engineering, vol. 15, p. 100473, Sep. 2022, doi: 10.1016/j.rineng.2022.100473.
[27] E. Maleki, S. Bagherifard, M. Bandini, and M. Guagliano, "Surface post-treatments for metal additive manufacturing: Progress, challenges, and opportunities," Addit Manuf, vol. 37, p. 101619, Jan. 2021, doi: 10.1016/j.addma.2020.101619.
[28] M. Salmi, "Additive Manufacturing Processes in Medical Applications," Materials, vol. 14, no. 1, p. 191, Jan. 2021, doi: 10.3390/ma14010191.
[29] Z. Jardon, J. Ertveldt, R. Lecluyse, M. Hinderdael, and L. Pyl, "Directed Energy Deposition roughness mitigation through laser remelting," Procedia CIRP, vol. 111, pp. 180–184, 2022, doi: 10.1016/j.procir.2022.08.042.
[30] G. Piscopo, A. Salmi, and E. Atzeni, "Influence of High-Productivity Process Parameters on the Surface Quality and Residual Stress State of AISI 316L Components Produced by Directed Energy Deposition," J Mater Eng Perform, vol. 30, no. 9, pp. 6691–6702, Sep. 2021, doi: 10.1007/s11665-021-05954-3.
[31] Kenneth Vartanian, Lucas Brewer, Karen Manley, and Tom Cobbs, "Powder Bed Fusion vs. Directed Energy Deposition benchmark study: mid-size part with simple geometry," Optomec Corporation, 3911 Singer Blvd. NE, Albuquerque, New Mexico, 87109 USA.
[32] M. Armstrong, H. Mehrabi, and N. Naveed, "An overview of modern metal additive manufacturing technology," J Manuf Process, vol. 84, pp. 1001–1029, Dec. 2022, doi: 10.1016/j.jmapro.2022.10.060.
[33] RJF. SILVA, "Fabrication of microtextures with varying hydrophilicity using µball nose in Ti6Al4V to improve cell adhesion," School of Engineering of São Carlos, University of São Paulo, São Carlos, 2022., São Carlos, 2022.
[34] M. A. F. Martinez et al., "Surface roughness of titanium disks influences the adhesion, proliferation, and differentiation of osteogenic properties derived from human," Int J Implant Dent, vol. 6, no. 1, p. 46, Dec. 2020, doi: 10.1186/s40729-020-00243-5.
[35] K. N. Hansson and S. Hansson, "Skewness and Kurtosis: Important Parameters in the Characterization of Dental Implant Surface Roughness—A Computer Simulation," ISRN Materials Science, vol. 2011, pp. 1–6, Oct. 2011, doi: 10.5402/2011/305312.
[36] P.-W. Peng et al., "Effects of Heat Treatment of Selective Laser Melting Printed Ti-6Al-4V Specimens on Surface Texture Parameters and Cell Attachment," Applied Sciences, vol. 11, no. 5, p. 2234, Mar. 2021, doi: 10.3390/app11052234.
[37] K. Zhang et al., "Pore evolution mechanisms during directed energy deposition additive manufacturing," Nat Commun, vol. 15, no. 1, p. 1715, Feb. 2024, doi: 10.1038/s41467-024-45913-9.